Numerical Analysis of Impulse-Radiating Antennas with Ellipsoidal Reflectors

Kangwook Kim [1], Waymond R. Scott, Jr. [2], Sang Wook Lee [1], and # Moongu Jeon [1]
[1] *Department of Mechatronics, Gwangju Institute of Science and Technology*
Gwangju, Republic of Korea, mkkim@gist.ac.kr, yashin96@gist.ac.kr, mgjeon@gist.ac.kr
[2] *School of Electrical and Computer Engineering, Georgia Institute of Science and Technology*
Atlanta, GA, USA, Waymond.Scott@ece.gatech.edu

Abstract

An impulse-radiating antenna (IRA) can effectively focus its radiation in the near field by using an ellipsoidal reflector. In this paper, three IRAs with ellipsoidal reflectors (elliptic IRAs) are numerically analyzed and compared with an IRA with a typical parabolic reflector (parabolic IRA). The ellipsoidal reflector is parameterized by the distance between the center of the reflector and its closest focus (F), the distance between the two optical foci (Φ), and the diameter of the reflector (D). The IRAs have the same F/D, i.e., 0.5, but different Φ/D's, i.e., 0.5, 1.0, and 1.5. The electric fields in the near-field region and the reflected voltage in the feeding transmission line are analyzed. The elliptic IRAs have a larger impulse and a smaller beam in the near-field region than does the parabolic IRA. The maximum impulse amplitude and the minimum beam width do not occur at the optical focus for the input pulse considered in this paper. The amplitudes of the tail waveform and the reflected voltage in the transmission line are increased.

1. INTRODUCTION

In a typical reflector-type impulse-radiating antenna (IRA), a spherical transverse electromagnetic (TEM) wave is guided by TEM feed arms and converted into an equi-phase aperture by a parabolic reflector [1], [2], [3], [4]. The aperture is focused at infinity in the geometrical optics sense, and the radiated waveform of the aperture at its optical focus is an impulse when it is driven by a step pulse. Thus, the IRA with a parabolic reflector (parabolic IRA) is capable of transmitting a temporally short pulse on boresight in the far-field region.

Recently, researchers have been considering IRAs for use in ground penetrating radar (GPR) systems because of the short pulse radiation capability [5], [6]. However, for most GPR systems, the target is close to the antennas. In this region, the impulse part of the waveform is not fully developed, so the performance of the IRA is degraded [7], [8].

In order to improve the performance of the IRA for this application, the aperture must be focused at a distance close to the antenna. This can be achieved by using a portion of an ellipsoid of revolution as a reflector [9]. An ellipsoid of revolution has two optical foci, and an optics ray originating at one focus arrives at the other focus with the same amount of delay after a single bounce at any point on the ellipsoid. Thus, the aperture formed by the ellipsoidal reflector is focused on the second focus.

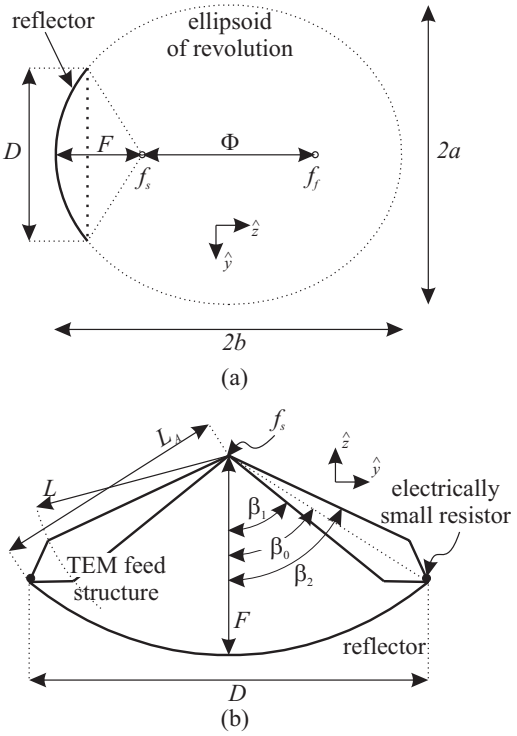

Fig. 1: Geometry of the elliptic IRA. (a) Ellipsoid of revolution and its two foci. (b) Schematic description of the elliptic IRA.

The characteristics of an IRA with an ellipsoidal reflector (elliptic IRA) over a wide bandwidth may be understood by a numerical model. Thus, in this paper, we investigate the characteristics of the elliptic IRAs by modeling the antennas numerically. The numerical model is developed using the method of moments code in EIGER [10], [11]. The performance of the numerical model using EIGER has been validated in [8].

2. MODELING OF THE IRAS

Consider the geometry shown in Fig. 1 (a). The dotted curve represents an ellipsoid of revolution whose equation may be

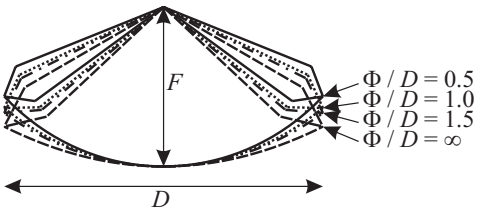

Fig. 2: Diagrams of the IRAs with $\Phi/D = 0.5$, 1.0, 1.5, and ∞. The diagrams are drawn on top of each other to show the differences in the geometries.

written as

$$\frac{x^2}{a^2} + \frac{y^2}{a^2} + \frac{z^2}{b^2} = 1, \quad a < b, \tag{1}$$

where the axis of revolution is the z-axis. The distance between the two foci (Φ) and the distance between focus f_s and its closest vertex (F) can be written in terms of a and b as:

$$\Phi = 2\sqrt{b^2 - a^2}, \quad F = b - \sqrt{b^2 - a^2}. \tag{2}$$

The reflector is the circular portion of diameter D around the vertex.

Three elliptic IRAs with $F/D = 0.5$ are modeled in this paper. Φ/D's for these IRAs are 0.5, 1.0, and 1.5. These elliptic IRAs are compared with a typical parabolic IRA ($\Phi/D = \infty$) whose numerical model has been developed in [8]. In [8], the numerical model was used to analyze the parabolic IRA with two pairs of TEM feed arms. Here, it is used to analyze the parabolic IRA with one pair of TEM feed arms. The dimensions of the elliptic IRAs and the parabolic IRA are summarized and compared in Table 1. The differences of the geometries are seen in Fig. 2, where the diagrams of the IRAs are drawn on top of each other.

Each IRA has a pair of conical coplanar plates as TEM feed arms. The apex of the TEM feed arms is placed at f_s, and the angles associated with the TEM feed arms (β_0, β_1, β_2) are such that the characteristic impedance is 400Ω within a spherical region of radius L centered at f_s [12], [13]. Outside the spherical region, each TEM feed arm is linearly tapered to an electrically-small 200Ω resistor, which connects the TEM feed arm to the reflector. The series resistance seen at the terminals of one pair of the TEM feed arms is 400Ω at zero frequency, so these resistors improve the input impedance of the antenna at low frequencies. The radius of the spherical region is chosen to be $L = F$ for all IRAs. This choice of L allows the positive reflection from the taper to cancel the negative reflection from the reflector at the apex [14]. Thus, the reflected voltage in the transmission line is lowered.

A computer program was written to generate the meshes of the elliptic IRAs for the numerical model. Because the IRAs have reflection symmetry across the x-z plane, half of the geometry can be replaced with a perfect electric conductor (PEC) plane placed perpendicular to the TEM feed arms. This improves the efficiency of the numerical model significantly.

The efficiency can be further improved by using a different mesh for each frequency, i.e., using a coarser mesh for a lower

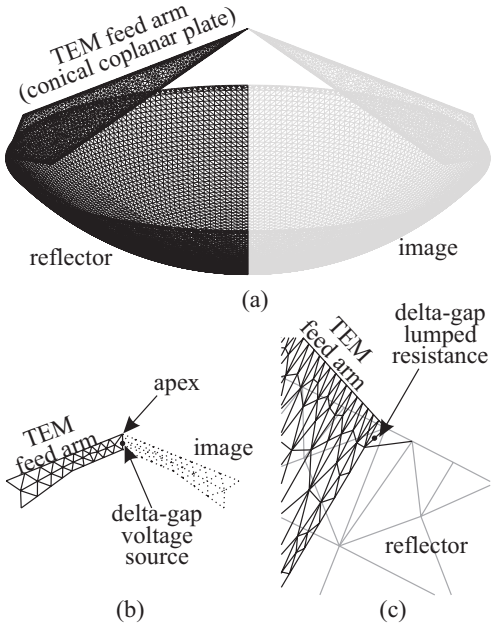

Fig. 3: The high frequency mesh for the IRA with $\Phi/D = 0.5$. (a) The mesh used for the numerical model and its image resulting from the PEC reflection symmetry. (b) Apex approximation. (c) TEM feed arm termination with an electrically small resistor.

frequency and a denser mesh for a higher frequency. In this paper, two meshes are used for each elliptic IRA to calculate the responses at 150 equally spaced points within normalized frequency range from $D/\lambda = 0.102$ to 15.3, where λ is the wavelength in freespace.[1] The meshes for the lower 75 frequencies contain 5233, 5117, and 4986 triangle elements, and the meshes for the higher 75 frequencies contain 10658, 10425, 10255 triangle elements for the IRAs with $\Phi/D = 0.5$, 1.0, and 1.5, respectively. Fig. 3 shows the high frequency mesh for the IRA with $\Phi/D = 0.5$ as an example. The approximation for the apex geometry and the approximation for the electrically small resistor are shown in Fig. 3 (b) and (c), respectively. The electrically small resistor is modeled using a 200Ω delta-gap lumped impedance model. A delta-gap voltage source is placed at the apex to excite the mesh.

The electric field integral equation with linear basis functions is used to solve for the mesh currents. The EIGER physics solver (EIGER Solve) was executed in parallel on the Beowulf cluster at the Electromagnetics/Acoustics Laboratory using the message passing interface (MPI) protocol to produce the mesh currents. The run times were approximately 79.0, 72.3, 66.8 hours for the IRAs with $\Phi/D = 0.5$, 1.0, and 1.5, respectively, using 32 computer nodes; each node is equipped with an AMD Athlon™ 2200+ processor. The electric fields are obtained by running the EIGER physics solver for sec-

[1]Note that the upper frequency limit was chosen because of computer run time considerations, not limits on the IRA. The chosen upper frequency limit gives us reasonable run times while giving us enough frequency content to see essentially all of the interesting interactions in the antennas. This upper frequency limit sets the minimum pulse parameters in the later graphs.

TABLE 1: DIMENSIONS OF THE IRAS.

Φ/D	F/D	L/D	L_A/D	β_0	β_1	β_2	Z_0
0.5	0.5	0.5	0.5732	60.72°	53.85°	68.08°	400Ω
1.0	0.5	0.5	0.5918	57.67°	51.03°	64.82°	400Ω
1.5	0.5	0.5	0.6005	56.37°	49.85°	63.44°	400Ω
∞	0.5	0.5	0.6250	53.13°	46.88°	59.94°	400Ω

ondary quantities (EIGER Analyze). The numerical results are valid for the half IRAs. The responses of the full IRAs can be obtained by simple algebraic manipulations of the quantities generated by the numerical model, i.e., doubling the input impedances and halving the currents and fields.

3. ANALYSIS

In this paper, each antenna is fed by a transmission line, which has the same characteristic impedance as the TEM feed arms. The responses in the frequency domain are transformed into the time domain for input voltage pulses incident in the transmission line. The input pulses considered in this paper are step-like and Gaussian pulses, which are defined as follows:

$$\text{Step-like:} \quad V(t) = V_0 \left\{ \frac{1}{2} + \frac{1}{2} \operatorname{erf}\left(k_1 \frac{t}{t_{10\text{-}90\%}} \right) \right\}, \qquad (3)$$

$$k_1 = 2 \operatorname{erf}^{-1}(0.8) \simeq 1.8124,$$

$$\text{Gaussian:} \quad V(t) = V_0 e^{-\ln 16 (t/t_{FWHM})^2}, \qquad (4)$$

where $\operatorname{erf}(t)$ is the error function, V_0 is the maximum amplitude of the pulse, and the pulse parameters $t_{10\text{-}90\%}$ and t_{FWHM} are the 10% – 90% rise time of the step-like pulse and the full-width half-maximum of the Gaussian pulse, respectively [15]. The waveforms and their frequency spectrums are shown in [8].

The readers may be most interested in the following characteristics of the IRAs with an ellipsoidal reflector: the waveforms radiated by the antenna in the near field, spot sizes illuminated by the antenna, and the voltage reflected back to the feed line. These characteristics are analyzed and compared with those of the IRA with a paraboloidal reflector in the following subsections.

A. Near-Field Waveforms

Fig. 4 shows electric fields of the antennas in the near-field region. In each graph, the electric fields (E_y/V_0) on the z-axis are plotted as a function of time for a step-like pulse with $t_{10\text{-}90\%}/\tau_a = 0.075$ and vertically displaced according to the observation distance. Here, the parameter $\tau_a = D/c$ is the time required by light to travel the length of the reflector diameter. For antennas with a finite Φ, the electric field at focus f_f is plotted with a dotted line.

The figure shows that the impulse is stronger for a smaller Φ in the near-field region. The impulse of the antenna with a smaller Φ grows faster and also decays faster. These are the expected results by focusing the aperture at distances close to the antenna. Note, however, that the maximum impulse amplitude does not occur at focus f_f because the electrical size of the aperture is small compared to the ratio Φ/D. It has been empirically found that for a square aperture of side length a, $a/\lambda \geq 25\Phi/a$ is required to result in the maximum amplitude close to focus f_f [16]. For a circular aperture, this requirement is approximately

$$\frac{D}{\lambda} \geq \frac{100}{\pi} \frac{\Phi}{D}. \qquad (5)$$

The minimum requirement corresponds to $D/\lambda \geq 15.9$, 31.8, and 47.7 for the IRAs with $\Phi/D = 0.5$, 1.0, and 1.5, respectively. These requirements are all higher than the frequency range we used in the numerical model (max $D/\lambda = 15.3$). The maximum impulse amplitude will occur close to focus f_f by using pulses with a faster rise time.

In Fig. 5, the envelope of the impulse amplitude ($\max E_y/V_0$) is plotted for each IRA for step-like pulses with $t_{10\text{-}90\%}/\tau_a = 0.075$ and 0.2. The envelopes with larger amplitudes are those for $t_{10\text{-}90\%}/\tau_a = 0.075$, and the envelopes with

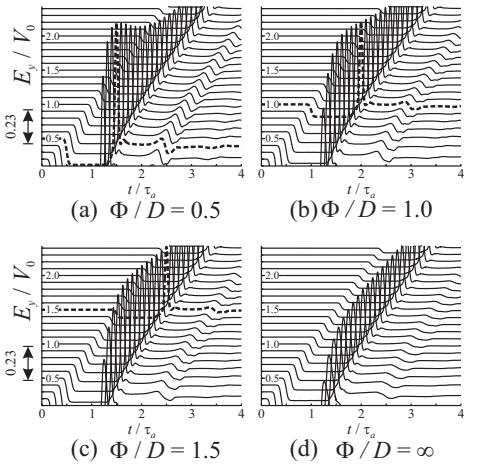

Fig. 4: Waterfall graphs of the electric fields (E_y/V_0) for the IRAs with $\Phi/D =$ (a) 0.5, (b) 1.0, (c) 1.5, and (d) ∞. The numbers on the lines are the normalized distance (r/D) for the lines.

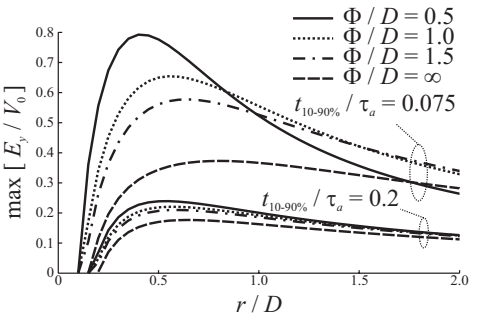

Fig. 5: Impulse envelopes (max E_y/V_0) for step-like pulses with $t_{10\text{-}90\%}/\tau_a = 0.075$ and 0.2.

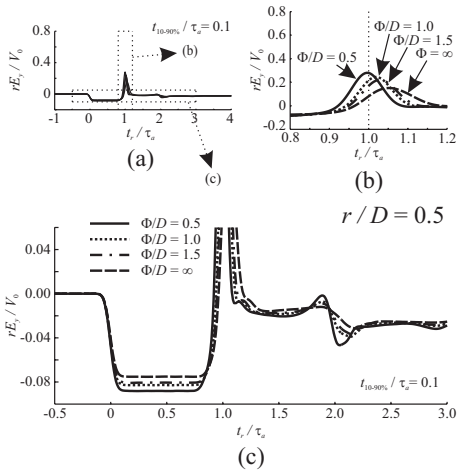

Fig. 6: Comparison of the electric fields at $r/D = 0.5$ for a step-like pulse with $t_{10\text{-}90\%}/\tau_a = 0.1$. Magnifications of the waveforms are shown in (b) and (c).

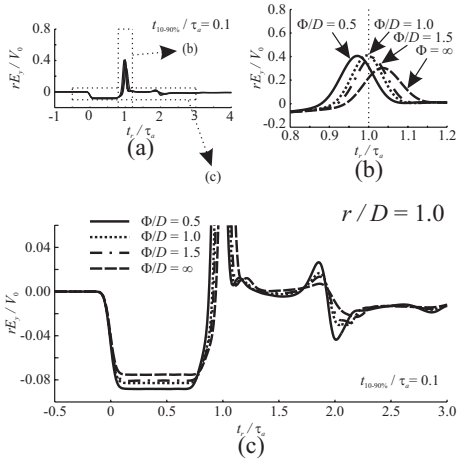

Fig. 7: Comparison of the electric fields at $r/D = 1.0$ for a step-like pulse with $t_{10\text{-}90\%}/\tau_a = 0.1$. Magnifications of the waveforms are shown in (b) and (c).

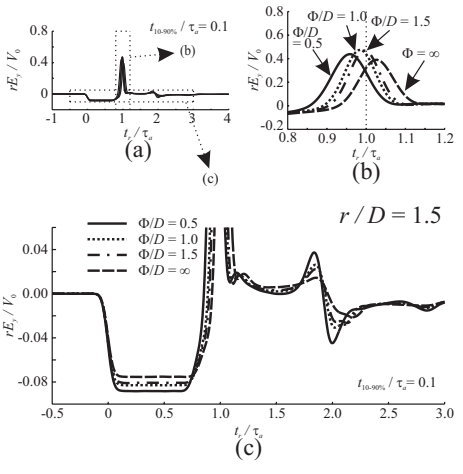

Fig. 8: Comparison of the electric fields at $r/D = 1.5$ for a step-like pulse with $t_{10\text{-}90\%}/\tau_a = 0.1$. Magnifications of the waveforms are shown in (b) and (c).

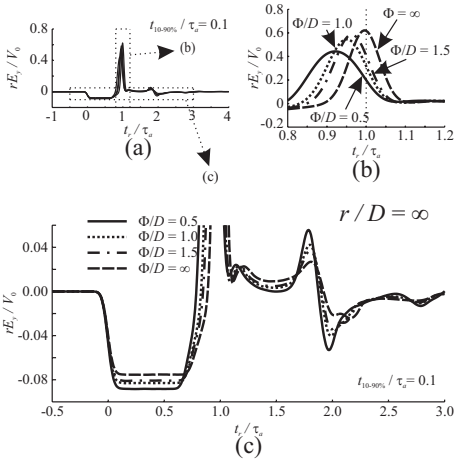

Fig. 9: Comparison of the electric fields at $r/D = \infty$ for a step-like pulse with $t_{10\text{-}90\%}/\tau_a = 0.1$. Magnifications of the waveforms are shown in (b) and (c).

smaller amplitudes are those for $t_{10\text{-}90\%}/\tau_a = 0.2$. As noted in Fig. 4, the impulse envelope for the IRA with a smaller Φ grows faster than the impulse envelope for the IRA with a larger Φ. It also decays faster after it reaches its maximum. For example, for $t_{10\text{-}90\%}/\tau_a = 0.075$, the impulse envelope for the IRA with $\Phi/D = 0.5$ grows faster and remains larger than those for other IRAs until $r/D \simeq 0.8$. After it reaches its maximum at $r/D \simeq 0.4$, it decays faster and becomes smaller than those for other IRAs after $r/D \simeq 1.8$.

For the case with $t_{10\text{-}90\%}/\tau_a = 0.2$, the amplitude of the impulse is only weakly dependent on Φ/D; this is due to the predominantly low-frequency content of the input pulse. Thus, one has to use a fast rising pulse to utilize the close-in range focusing characteristic of the ellipsoidal reflector.

In Figs. 6 – 9, the electric fields of the IRAs are compared on the rotational axis of the reflector at $r/D = 0.5$, 1.0, 1.5, and ∞, which are the points f_f of the four IRAs. Here, the graphs are plotted for a step-like pulse with $t_{10\text{-}90\%}/\tau_a = 0.1$ as functions of retarded time $t_r = t - r/c$, where r is the distance from the apex (f_s) to the observer. In each figure, the impulses are magnified in (b), and the prepulses and postpulses are magnified in (c).

At each observation distance, the impulse centered at $t_r/\tau_a = 1.0$ is the one from the IRA with Φ equal to the observation distance ($\Phi = r$). The impulse appears earlier than $t_r/\tau_a = 1.0$ for the IRAs with $\Phi > r$ and later than $t_r/\tau_a = 1.0$ for the IRAs with $\Phi < r$. Because the IRA is focused at f_f, the signal from any point on the reflector arrives at f_f with the same amount of time delay. At a point other than f_f, the signals from different points on the reflector arrive with different time delays. For example, for the IRA with $\Phi/D = 0.5$, the signal from each point on the reflector arrives

at $r/D = 0.5$ at $t_r/\tau_a = 1.0$. Thus, the peak occurs exactly at $t_r/\tau_a = 1.0$. However at $r/D = 1.0$, the signal from the center of the reflector arrives at $t_r/\tau_a = 1.0$ while the signal from the edge of the reflector arrives at $t_r/\tau_a = 0.948$. Thus, the peak occurs between $t_r/\tau_a = 0.948$ and $t_r/\tau_a = 1.0$.

One would think the amplitude of the impulse for the IRA with $\Phi = r$ should be larger at $r = \Phi$ than those for the other IRAs because of the focusing; this is correct in Figs. 6, 7, and 9. However, it is not correct in Fig. 8, where the impulse for $\Phi/D = 1.0$ is the largest. The reason for this was explained earlier and is due to the electrical size of the aperture. If the pulse rise time is much shorter than the time it takes by light to travel across the aperture ($t_{10\text{-}90\%} << \tau_a$), the impulse for the IRA with $\Phi = r$ will be the largest at $r = \Phi$.

For each antenna, the prepulse amplitudes are the same irrespective of the observation distance. The reason for this is that the prepulse originates at one point (apex) and has a $1/r$ dependence. Thus, the amplitude becomes constant when it is normalized by V_0/r. However, at any observation point, the prepulse for the IRA with a smaller Φ is larger than that for the IRA with a larger Φ because the TEM feed arms are more inclined toward the boresight direction guiding more energy toward the boresight direction.

The waveform at $t_r/\tau_a \simeq 1.2$ is due to the re-radiation of the signal taking the apex – resistor – apex path. The waveform at $t_r/\tau_a \simeq 2.0$ is due to a number of internally reflected signals, and it dominates the tail waveform. This waveform is larger for the IRA with a smaller Φ. This can be a drawback of the elliptic IRA for use in a remote sensing application because the signal from the target can be obscured by a large tail.

B. Spot Sizes

Fig. 10 shows the spot sizes of the IRAs for a step-like pulse with $t_{10\text{-}90\%}/\tau_a = 0.075$. To determine a spot size, an imaginary observation plane that is normal to the z-axis is placed at a distance, where the distribution of the impulse amplitude (max E_y) is recorded. Then, the full-width half-maximum of the impulse amplitude distribution on the plane is taken as the spot size. In Fig. 10, half-maximum points are plotted in the E- and H-planes.

The spot sizes for the elliptic IRAs are significantly smaller compared to the spot size for the parabolic IRA at a distance closer than $r/D \simeq 1.0$. As the observer moves out, the spot size for the elliptic IRA diverges more rapidly than that for the parabolic IRA. Note that the minimum waist does not occur at f_f because of the finite aperture size. Note also that the spot size is smaller in the E-plane and larger in the H-plane.

C. Reflected Voltages in the Feed Line

In Fig. 11 (a), (b), the reflected voltages in the feeding transmission line are compared as functions of time for a step-like pulse with $t_{10\text{-}90\%}/\tau_a = 0.1$ and a Gaussian pulse with $t_{FWHM}/\tau_a = 0.1$. The magnifications of the waveforms surrounded by the boxes are shown in Fig. 11 (c), (d). In Fig. 11 (a), (b), the first pulse around $t/\tau_a = 0$ is the reflection

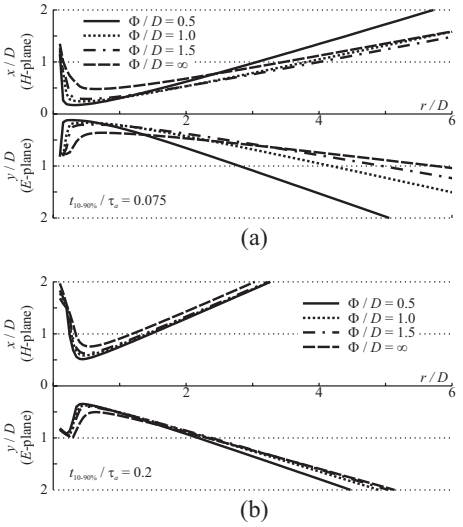

Fig. 10: Illuminated impulse spot sizes as functions of normalized distance. The lines in the upper half of each graph are those in the H-plane and the lines in the lower half are those in the E-plane. The input pulses are step-like pulses with (a) $t_{10\text{-}90\%}/\tau_a = 0.075$ and (b) $t_{10\text{-}90\%}/\tau_a = 0.2$.

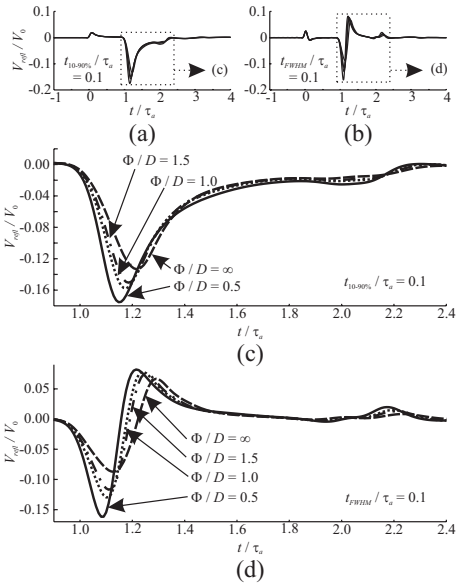

Fig. 11: Voltage reflected into the feeding transmission line for (a) a step-like pulse and (b) a Gaussian pulse with $t_{10\text{-}90\%}/\tau_a = t_{FWHM}/\tau_a = 0.1$. The waveforms surrounded by the boxes in (a), (b) are magnified in (c), (d).

from the junction between the feeding transmission line and the antenna (f_s). This reflection is due to the approximation made to the apex geometry (Fig. 3 (b)). The first possible disturbance after this reflection is the superposition of the positive signal from the TEM feed arm and negative signal from the reflector; both signals begin at $t/\tau_a = 1.0$. In Fig. 11 (a), the waveform is not exactly zero over the time interval $0 < t/\tau_a < 1.0$ because of a small error in the characteristic impedance of the TEM feed arms predicted by the numerical

model ($\sim 1\%$).

The waveforms have the maximum amplitudes around $t/\tau_a = 1.2$. The maximum amplitude increases with decreasing Φ. Because the reflector with a smaller Φ focuses the wave at a distance closer to the apex, more negative current is induced on the TEM feed arms at the apex. In addition, the maximum amplitude occurs earlier in time with decreasing Φ. The reason for this is that the diffracted signal from the reflector edge arrives earlier as Φ decreases, and this signal contributes to the waveform positively. Because the path length of the diffracted signal to the apex (L_A) is shorter for the IRA with smaller Φ, the cancellation begins earlier.

4. CONCLUSION

The IRAs with ellipsoidal reflectors were numerically analyzed and compared with the IRA with a parabolic reflector. The focal length to diameter ratios of the reflectors were all $F/D = 0.5$. The shape of an ellipsoidal reflector was determined by the parameter Φ, which was the distance between the two optical foci of the ellipsoid.

The elliptic IRAs produced stronger impulses and narrower spot sizes in the near-field region than does the parabolic IRA. This feature of the elliptic IRA may be useful in close-in sensing applications. However, the maximum impulse amplitude and the minimum spot size did not occur at f_f of the ellipsoidal reflector for pulses used in this paper. To have the maximum impulse amplitude at f_f, one has to use a pulse with a faster rise time.

The elliptic IRAs had larger tail waveforms than the parabolic IRA. The tail waveform can be lowered by using an offset geometry [17]. The elliptic IRA also had larger reflected voltages in the transmission line. The reason for this is that the negative signal from the reflector was stronger with decreasing Φ. The reflected voltage can be lowered by refining the shape of the TEM feed arm taper so that the positive signal from the taper is increased [18]. This increase in the positive signal will cancel the reflector signal, and therefore the reflected voltage will be lowered. Another possibility is to use distributed impedance at the TEM feed arm termination as shown in [19] for a parabolic reflector. In [19], the time domain reflectometry measurement data was seen to be quite flat, and therefore the reflected voltage in the transmission line is low.

REFERENCES

[1] C. E. Baum and E. G. Farr, "Impulse radiating antennas," in *Ultra-Wideband, Short Pulse Electromagnetics*. H. Bertoni *et al.,* Eds. New York: Plenum, 1993, pp. 139–147.

[2] E. G. Farr, C. E. Baum, and C. J. Buchenauer, "Impulse radiating antennas, part II," in *Ultra-Wideband, Short Pulse Electromagnetics 2*. L. Carin and L. B. Felsen, Eds. New York: Plenum, 1995, pp. 159–170.

[3] D. V. Giri, H. Lackner, I. D. Smith, D. W. Morton, C. E. Baum, J. R. Marek, W. D. Prather, and D. W. Scholfield, "Design, fabrication, and testing of a paraboloidal reflector antenna and pulser system for impulse-like waveforms," *IEEE Trans. Plasma Sci.*, vol. 25, no. 2, pp. 318–326, Apr. 1997.

[4] C. E. Baum, E. G. Farr, and D. V. Giri, "Review of impulse-radiating antennas," in *Reviw of Radio Science 1996-1999*. W. R. Stone, Ed. Oxford University Press, 1999, ch. 16, pp. 403–439.

[5] E. G. Farr and L. H. Bowen, "Impulse radiating antennas for mine detection," in *Detection and Remediation Technologies for Mines and Minelike Targets VI, Proc. SPIE*, vol. 4394, Apr. 2001, pp. 680–691.

[6] J. R. R. Pressley, D. Pabst, G. Sower, L. Nee, B. Green, and P. Howard, "Ground standoff mine detection system (GSTAMIDS) engineering, manufacturing and development (EMD) block 0," in *Detection and Remediation Technologies for Mines and Minelike Targets VI, Proc. SPIE*, vol. 4394, Apr. 2001, pp. 1190–1200.

[7] G. Sower, J. Eberly, and E. Christy, "GSTAMIDS ground-penetrating radar: hardware description," in *Detection and Remediation Technologies for Mines and Minelike Targets VI, Proc. SPIE*, vol. 4394, Apr. 2001, pp. 651–661.

[8] K. Kim and W. R. Scott, Jr., "Numerical analysis of the impulse-radiating antenna," Sensor and Simulation Notes #474, June 3, 2003.

[9] K. Hirasawa, K. Fujimoto, T. Uchikura, S. Hirafuku, and H. Naito, "Power focusing characteristics of ellipsoidal reflector," *IEEE Trans. Antennas Propagat.*, vol. AP-32, no. 10, pp. 1033–1039, Oct. 1984.

[10] R. M. Sharpe, J. B. Grant, N. J. Champagne, W. A. Johnson, R. E. Jorgenson, D. R. Wilton, W. J. Brown, and J. W. Rockway, "EIGER: Electromagnetic interactions generalized," in *IEEE AP-S Int'l Symp. Digest, Quebec, Canada*, Jul. 1997, pp. 2366–2369.

[11] Lawrence Livermore National Laboratory. (2001, March 5) EIGER - A Revolution in Computational Electromagnetics. [Online]. Available: http://cce.llnl.gov/eiger/

[12] E. G. Farr and C. E. Baum, "Prepulse associated with the TEM feed of an impulse radiating antenna," Sensor and Simulation Notes #337, Mar. 1992.

[13] E. G. Farr, "Optimizing the feed impedance of impulse radiating antennas, Part I: Reflector IRAs," Sensor and Simulation Notes #354, Jan. 1993.

[14] C. E. Baum, "Some topics concerning feed arms of reflector IRAs," Sensor and Simulation Notes #414, Oct. 31, 1997.

[15] M. Abramowitz and I. A. Stegun, *Handbook of Mathematical Functions with Formulas, Graphs, and Mathematical Tables*. New York: Dover, 1972.

[16] J. W. Sherman, III, "Properties of focused apertures in the Fresnel region," *IRE Trans. Antennas Propagat.*, vol. AP-10, no. 4, pp. 399–408, Jul. 1962.

[17] K. Kim and W. R. Scott, Jr., "Analysis of an offset impulse-radiating antenna," Sensor and Simulation Notes #476, June 16, 2003.

[18] K. Kim, "Numerical and experimental investigation of impulse-radiating antennas for use in sensing applications," Ph.D. dissertation, Georgia Institute of Technology, April 2003.

[19] M. Abdalla, M. Skipper, D. V. Giri, H. La Valley, T. Smith, D. McLemore, J. Burger, R. Torres, T. Tran, W. Prather, and C. E. Baum, "Evaluation of the terminating impedance in the conical-line feed of the 6-foot IRA," Prototype IRA Memos #8, Apr. 15, 2001.